Modeling Large Planar Deflections of Flexible Beams in Compliant Mechanisms Using Chained Beam-Constraint-Model[1]

Fulei Ma
School of Electro-Mechanical Engineering,
Xidian University,
Xi'an, Shaanxi 710071, China

Guimin Chen[2]
School of Electro-Mechanical Engineering,
Xidian University,
Xi'an, Shaanxi 710071, China
e-mail: guimin.chen@gmail.com

Modeling large deflections has been one of the most fundamental problems in the research community of compliant mechanisms. Although many methods are available, there still exists a need for a method that is simple, accurate, and can be applied to a vast variety of large deflection problems. Based on the beam-constraint model (BCM), we propose a new method for modeling large deflections called chained BCM (CBCM), which divides a flexible beam into a few elements and models each element by BCM. The approaches for determining the strain energy stored in a deflected beam and the stress distributed on it are also presented within the framework of CBCM. Several typical examples were analyzed and the results show CBCMs capabilities of modeling various large deflections of flexible beams in compliant mechanisms. Generally, CBCM can serve as an efficient and versatile tool for solving large deflection problems in a variety of compliant mechanisms. [DOI: 10.1115/1.4031028]

1 Introduction

Compliant mechanisms have been playing increasingly important roles in high-precision manufacturing [1], scientific instruments, minimally invasive surgeries, and microelectromechanical systems, etc. Unlike rigid-body mechanisms, compliant mechanisms achieve at least some of their mobility through the deflections of flexible members, thus can provide precise and frictionless motion in their workspace [2,3]. In compliant mechanisms, compliant segments usually undergo large deflections; therefore, modeling the large deflections has been one of the most fundamental problems in the research community [3,4]. Initially, straight beams are the most commonly used flexible segments in compliant mechanisms due to their simplicity as well as their binary constraint property [5]. For this reason, only initially straight beams are considered in this paper.

There have been many methods available for analyzing the large deflection problems [6], e.g., the pseudo-rigid-body method [3], the elliptic integral solution (EIS) [7], the circle-arc method [8], the Adomian decomposition method [9,10], and the chain algorithm [11], as will be reviewed in Sec. 2. However, there still exists a need for a method that is simple, accurate, and can be applied to a vast variety of large deflection problems.

Originally, the BCM [12] was developed for the purpose of accurately predicting the behaviors of flexible beams in their intermediate deflection range. It has been demonstrated that BCM can accurately capture the relevant nonlinearities when deflections are within 10% of the beam length [12,13]. What is more, BCM is simple, parametric, and closed-form. To take these advantages of BCM for modeling large deflection problems, in this work, we proposed a BCM-based method called CBCM, in which a flexible beam is divided into a few elements and each element is modeled by BCM. The major advantages of CBCM are highlighted in the following:

1. Because each BCM element is capable of accurately modeling intermediate deflections, CBCM requires much fewer elements than other discretization-based methods utilizing linear elements (e.g., the chain algorithm and the circle-arc method) to obtain desired accuracy.
2. The maximum compressive load in BCM is $P = -\pi^2 EI/(4L^2)$ (all the compliance terms exhibit a singularity at this value), which corresponds to the first fixed-free beam buckling mode [12]. CBCM eliminates this limitation of BCM through discretization. For example, if a beam is discretized into two elements of equal length (the length of each element is $L/2$), then the corresponding maximum compressive load of the model becomes $4P$. This indicates that CBCM is capable of predicting complicated deflection configurations that correspond to higher buckling modes [14] and carry multiple inflection points [7].
3. Because BCM captures elastokinematic effects [12], the resulting CBCM outperforms those methods that ignore the axial strain (e.g., the EIS, the circular-arc method [8], and the Adomian decomposition method [9,10]) when the axial load is significant.

It has also been demonstrated that shear effect can be incorporated in BCM (TBCM) [15]. Nevertheless, for a stubbly beam where shear effects are significant [16,17], the deflection is always small thus a single TBCM element can yield accurate results, that is to say, generally no discretization is required.

The rest of this paper is organized as follows: Sec. 2 presents a brief summary of various methods for modeling large deflections of flexible beams. Section 3 reviews the basic equations of BCM [12] and presents the idea and the basic formulation of CBCM.

[1]Paper presented at the ASME 2014 Design Engineering Technical Conferences and Computers and Information in Engineering Conference (DETC2014), Aug. 17–20, 2014, Buffalo, NY.
[2]Corresponding author.
Manuscript received April 6, 2015; final manuscript received June 12, 2015; published online November 24, 2015. Assoc. Editor: Larry L. Howell.

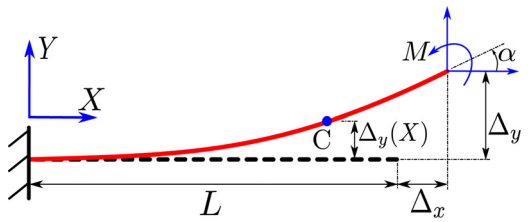

Fig. 1 A simple beam subject to combined force and moment loads at its free end

Examples are given in Sec. 4 to illustrate the capabilities of CBCM for modeling various large deflections of flexible beams in compliant mechanisms. The concluding remarks are made in Sec. 5.

2 Methods for Modeling Large Deflections: A Survey

As aforementioned, many methods have been proposed and developed for analyzing the large deflection problems of flexible beams in compliant mechanisms. This section briefly reviews and roughly compares some of these methods.

The EIS [3,18] represents the exact solution to the Bernoulli–Euler beam equation but its derivation and implementation are quite intricate. The use of the solution is straightforward only if the end slope and the load parameters are given; otherwise, a numerical iterative process is required to solve the deflections and the process may be sensitive to the initial guess of the unknown parameters. The comprehensive elliptic integral solution (CEIS) derived in Ref. [7] is capable of solving the large deflections of beams with multiple inflection points and subject to any kinds of load cases and locating multiple possible solutions. Holst et al. [14] superposed axial deflection on the EIS and used it to solve the deflections of fixed-guided beams.

The pseudo-rigid-body model (PRBM) method [3,19,20], which approximates the nonlinear deflection as motion of rigid links, provides an effective (although less accurate) way for design and analysis of compliant mechanisms. Although PRBM suffers from inaccuracies of modeling large deflections that carry inflection points [19,21], PRBM is particularly useful in the synthesis and the early design phase of compliant mechanisms.

Kramer and Saxena [22] employed a numerical integration technique based on Gauss–Chebyshev quadrature formulae for solving the Bernoulli–Euler beam equation. Banerjee et al. [10] presented a semi-analytical method known as Adomian decomposition to determine large deflection of a cantilever beam under arbitrary end loading conditions. Tolou and Herder [9] further developed the Adomian decomposition method for large deflections in compliant mechanisms. Lan [23] presented a method combining the global coordinate model with an incremental linearization approach, which transforms the nonlinear deflection problem into a sequence of linear problems.

There are also a few discretization-based methods available for large deflection modeling. The chain algorithm discretizes a beam into small elements, treats each element as a small-deflection beam cantilevered at the end of the previous element, and analyses each element in succession [3]. Campanile and Hasse [8] proposed a circle-arc method which uses a similar discretization technique as that used in the chain algorithm but approximates the deflection configuration of each element by a circular arc. The nonlinear finite-element analysis (FEA) is another discretization-based method (the deflection of each element is approximated by a polynomial interpolation function) that has been frequently used for modeling large deflections in compliant mechanisms. FEA can be applied to various large deflection problems but often predicts the wrong bucking modes for axial-force dominated load conditions [14]. CBCM is also classified as a discretization-based method.

3 CBCM

3.1 BCM. Figure 1 shows a simple beam subject to transverse force F, axial force P, and moment M at its free end, resulting in axial and transverse deflections δ_x and δ_y and end slope α. The parameters of the beam include: the length L, the in-plane thickness t, the out-of-plane thickness w, and the Young's modulus of the material E. $I = wt^3/12$ represents the area moment of inertia of the beam cross section. BCM models the load–deflection relations of the beam using the following parametric and closed-form equations [24]:

$$\begin{bmatrix} f \\ m \end{bmatrix} = \begin{bmatrix} g_{11} & g_{12} \\ g_{21} & g_{22} \end{bmatrix} \begin{bmatrix} \delta_y \\ \alpha \end{bmatrix} + p \begin{bmatrix} p_{11} & p_{12} \\ p_{21} & p_{22} \end{bmatrix} \begin{bmatrix} \delta_y \\ \alpha \end{bmatrix} + p^2 \begin{bmatrix} q_{11} & q_{12} \\ q_{21} & q_{22} \end{bmatrix} \begin{bmatrix} \delta_y \\ \alpha \end{bmatrix} \tag{1}$$

$$\delta_x = \frac{t^2 p}{12L^2} - \frac{1}{2} \begin{bmatrix} \delta_y & \alpha \end{bmatrix} \begin{bmatrix} u_{11} & u_{12} \\ u_{21} & u_{22} \end{bmatrix} \begin{bmatrix} \delta_y \\ \alpha \end{bmatrix} - p \begin{bmatrix} \delta_y & \alpha \end{bmatrix} \begin{bmatrix} v_{11} & v_{12} \\ v_{21} & v_{22} \end{bmatrix} \begin{bmatrix} \delta_y \\ \alpha \end{bmatrix} \tag{2}$$

in which all the load parameters and the deflection parameters are normalized with respect to the beam parameters and given as

$$m = \frac{ML}{EI}, \quad f = \frac{FL^2}{EI}, \quad p = \frac{PL^2}{EI}, \quad \delta_y = \frac{\Delta_y(L)}{L}, \quad \delta_x = \frac{\Delta_x(L)}{L}, \quad x = \frac{X}{L} \tag{3}$$

and the coefficients g's, p's, q's, u's, and v's are nondimensional beam characteristic coefficients listed in Table 1. These matrix terms are all symmetric. In addition, the strain energy stored in the deflected beam can be obtained as [25]

$$v = \frac{VL}{EI} = \frac{1}{2}\frac{t^2 p^2}{12L^2} + \frac{1}{2} \begin{bmatrix} \delta_y & \alpha \end{bmatrix} \begin{bmatrix} g_{11} & g_{12} \\ g_{21} & g_{22} \end{bmatrix} \begin{bmatrix} \delta_y \\ \alpha \end{bmatrix} - \frac{1}{2} p^2 \begin{bmatrix} \delta_y & \alpha \end{bmatrix} \begin{bmatrix} q_{11} & q_{12} \\ q_{21} & q_{22} \end{bmatrix} \begin{bmatrix} \delta_y \\ \alpha \end{bmatrix} \tag{4}$$

in which v is the normalized strain energy with respect to the beam parameters given as

$$v = \frac{VL}{EI}$$

and V is the strain energy.

The above equations of BCM only concern the relationships between the deflections and the loads of the beam. However, sometimes the deflected configuration of the beam is required. In

Table 1 Beam characteristic coefficients of BCM matrices [24] (note that the matrices are symmetric and *p*'s = *u*'s and *q*'s = *v*'s)

g_{11}	$g_{12} = g_{21}$	g_{22}	$p_{11} = u_{11}$	$p_{12} = p_{21} = u_{12} = u_{21}$	$p_{22} = u_{22}$	$q_{11} = v_{11}$	$q_{12} = q_{21} = v_{12} = v_{21}$	$q_{22} = v_{22}$
12	−6	4	6/5	−1/10	2/15	−1/700	1/1400	−11/6300

this case, the following equations providing the deflections at any point on the beam might be useful:

$$u_x(x) = \frac{t^2 x}{12} p - \begin{bmatrix} f & m \end{bmatrix} \begin{bmatrix} c_{11} & c_{12} \\ c_{21} & c_{22} \end{bmatrix} \begin{bmatrix} f \\ m \end{bmatrix}$$
$$\begin{bmatrix} u_y(x) \\ \theta(x) \end{bmatrix} = \begin{bmatrix} k_{11} & k_{12} \\ k_{21} & k_{22} \end{bmatrix} \begin{bmatrix} f \\ m \end{bmatrix} \tag{5}$$

where $x \in [0, 1]$ and k's and c's for $p > 0$ ($r = \sqrt{p}$) are given as

$$k_{11} = \frac{\tanh r}{r^3}[\cosh(rx) - 1] - \frac{\sinh(rx)}{r^3} + \frac{x}{r^2}$$
$$k_{12} = \frac{\cosh(rx) - 1}{r^2 \cosh r}$$
$$k_{21} = \frac{1 - \cosh(rx) + \tanh r \sinh(rx)}{r^2}$$
$$k_{22} = \frac{\sinh(rx)}{r \cosh r}$$
$$c_{11} = \frac{\begin{bmatrix} 4rx + 2rx\cosh(2r) - 4\sinh(rx - 2r) - 4\sinh(rx) \\ -\sinh(2r - 2rx) - 3\sinh(2r) \end{bmatrix}}{8r^5 \cosh^2 r}$$
$$c_{12} = c_{21} = \frac{\begin{bmatrix} 4\cosh(rx) - 2\cosh^2(rx) \\ +\tanh r(\sinh(2rx) - 2rx) - 2 \end{bmatrix}}{8r^4 \cosh r}$$
$$c_{22} = \frac{\sinh(2rx) - 2rx}{8r^3 \cosh^2 r}$$

and for $p < 0$ ($r = \sqrt{-p}$), k's and c's are given as

$$k_{11} = \frac{\sin(rx)}{r^3} - \frac{x}{r^2} - \frac{\tan r}{r^3}(\cos(rx) - 1)$$
$$k_{12} = \frac{1 - \cos(rx)}{r^2 \cos r}$$
$$k_{21} = \frac{\cos(rx) + \tan r \sin(rx) - 1}{r^2}$$
$$k_{22} = \frac{\sin(rx)}{r \cos r}$$
$$c_{11} = \frac{\begin{bmatrix} 4rx + 2rx\cos(2r) - 4\sin(rx - 2r) - 4\sin(rx) \\ -\sin(2r - 2rx) - 3\sinh(2r) \end{bmatrix}}{8r^5 \cos^2 r}$$
$$c_{12} = c_{21} = \frac{\begin{bmatrix} 4\cos(rx) - 2(\cos(rx))^2 \\ -\tan r[\sin(2rx) - 2rx] - 2 \end{bmatrix}}{8r^4 \cos r}$$
$$c_{22} = \frac{2rx - \sin(2rx)}{8r^3 \cos^2 r}$$

Once $u_y(x)$ is obtained, the maximum normal stress at position x (occurs at outermost fibers of this cross section) due to bending can be expressed as

$$\sigma_b(x) = \frac{M(x)t/2}{I} = E\frac{u_y''(x)t}{2L} \tag{6}$$

in which for $p > 0$ ($r = \sqrt{p}$), $u_y''(x)$ is expressed as

$$u_y''(x) = \frac{\tanh r \cosh(rx) - \sinh(rx)}{r} f + \frac{\cosh(rx)}{\cosh r} m$$

while for $p < 0$ ($r = \sqrt{-p}$), $u_y''(x)$ as

$$u_y''(x) = \frac{\tan r \cos(rx) - \sin(rx)}{r} f + \frac{\cos(rx)}{\cos r} m$$

The normal stress due to the axial force P can be estimated as

$$\sigma_t(x) = \frac{|P|}{A} = E\frac{|p|t^2}{12L^2} \tag{7}$$

which is uniformly distributed over the cross section and along the beam. Consequently, the resultant maximum stress at position x can be determined by superposition

$$\sigma(x) = \sigma_b(x) + \sigma_t(x) \tag{8}$$

3.2 CBCM. Figure 2 shows a cantilever beam deflected by an end transverse force F_o, an end axial force P_o, and an end moment M_o. Parameters θ_o, X_o, and Y_o denote the tip slope, the horizontal (the x-axis), and vertical (the y-axis) tip deflections of the beam, respectively.

CBCM discretizes the beam into several elements and models each element using BCM in succession. Suppose the beam is divided into N elements with equal length. For the ith ($1 \le i \le N$) element, its local coordinate frame ($O_i x_i y_i$) is attached to and moves along with the free end of $(i-1)$th element, i.e., node $(i-1)$. It should be noted that the first element was fixed to the ground at node 0 and the free end of the beam is node N. We use f_i, p_i, and m_i to denote the transverse force, the axial force, and the end moment applied on the ith element at node i with respect to its local coordinate frame, and δ_{xi}, δ_{yi}, and α_i denote the corresponding axial and transverse deflections and the end slope, respectively. The static equilibrium equations of the ith element can be expressed as

$$\begin{bmatrix} f'_{i-1} \\ p'_{i-1} \\ m'_{i-1} \end{bmatrix} = \begin{bmatrix} 1 & 0 & 0 \\ 0 & 1 & 0 \\ (1 + \delta_{xi}) & -\delta_{yi} & 1 \end{bmatrix} \begin{bmatrix} f_i \\ p_i \\ m_i \end{bmatrix} \tag{9}$$

where f'_{i-1}, p'_{i-1}, and m'_{i-1} are the transverse and axial forces and the end moment applied by the $(i-1)$th element to the ith element, respectively. As the ith element goes through a rigid-body rotation α_{i-1} along with the deflection of the $(i-1)$th element, we have

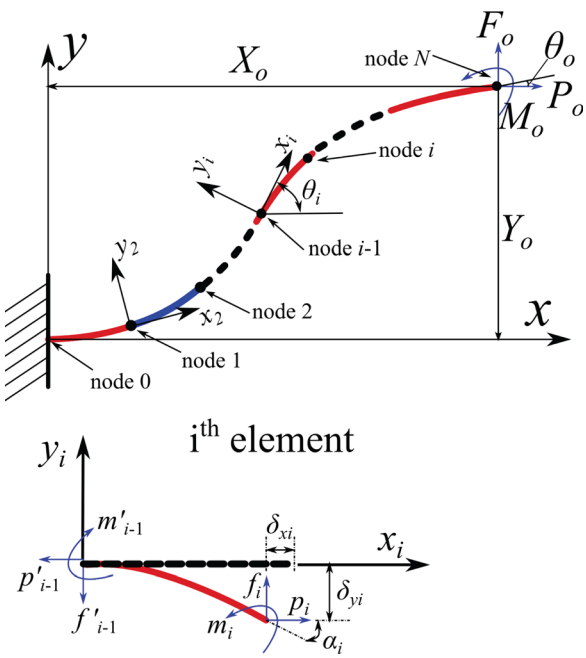

Fig. 2 Discretization

$$\begin{bmatrix} f_{i-1} \\ p_{i-1} \\ m_{i-1} \end{bmatrix} = \begin{bmatrix} \cos\alpha_{i-1} & -\sin\alpha_{i-1} & 0 \\ \sin\alpha_{i-1} & \cos\alpha_{i-1} & 0 \\ 0 & 0 & 1 \end{bmatrix} \begin{bmatrix} f'_{i-1} \\ p'_{i-1} \\ m'_{i-1} \end{bmatrix} \tag{10}$$

The rotation of the coordinate frame of the ith element with respect to the global coordinate frame, denoted by θ_i (note that $\theta_1 = 0$), can be expressed as

$$\theta_i = \sum_{1}^{i-1} \alpha_i \tag{11}$$

The load equilibrium equations for the ith ($i = 2, \ldots, N$) element can be rewritten from Eqs. (9) and (10) as (totally $3(N-1)$ equations)

$$\begin{bmatrix} \cos\theta_i & -\sin\theta_i & 0 \\ \sin\theta_i & \cos\theta_i & 0 \\ (1+\delta_{xi}) & -\delta_{yi} & 1 \end{bmatrix} \begin{bmatrix} f_i \\ p_i \\ m_i \end{bmatrix} = \begin{bmatrix} f_1 \\ p_1 \\ m_{i-1} \end{bmatrix} \tag{12}$$

in which the following relationships hold for the normalized end loads (note that f_1 is parallel to f_o and p_1 is parallel to p_o):

$$f_o = \frac{F_o L^2}{EI} = N^2 f_1; \quad p_o = \frac{P_o L^2}{EI} = N^2 p_1; \quad m_o = \frac{M_o L}{EI} = N m_N \tag{13}$$

The geometric constraint equations of the entire beam can be written as (three equations)

$$\begin{cases} \sum_{i=1}^{N-1} \left[\begin{bmatrix} \cos\theta_i & -\sin\theta_i \\ \sin\theta_i & \cos\theta_i \end{bmatrix} \begin{bmatrix} L_i(1+\delta_{xi}) \\ L_i\delta_{yi} \end{bmatrix} \right] = \begin{bmatrix} X_o \\ Y_o \end{bmatrix} \\ \theta_N + \alpha_N = \theta_o \end{cases} \tag{14}$$

where L_i is the length of the ith element and $L_i = L/N$ for equal discretization.

The geometric constraint equations given in Eq. (14) and the load equilibrium equations given in Eq. (12), together with the BCM equations for each element given in Eqs. (1) and (2), constitute the CBCM equations of the beam. CBCM eliminates the singularity at $P = -\pi^2 EI/(4L^2)$ of BCM through discretization, making the CBCM equations well-conditioned. Among three load parameters P_o, F_o, and M_o and three deflection parameters X_o, Y_o, and θ_o, given any set of three parameters, the other three parameters can be obtained by numerically solving the CBCM equations. After solving the CBCM equations, Eqs. (5)–(8) can be used if the deflected shape, the strain energy, and the maximum stress of the beam are required.

The total strain energy V_T stored in the beam can be obtained by adding the strain energy in each element

$$V_T = \sum_{1}^{N} \frac{v_i * EI}{L_i} \tag{15}$$

where v_i is determined by Eq. (4) in the element's coordinate frame.

4 Examples

In this section, a few examples are presented to demonstrate the effectiveness of CBCM in dealing with flexible cantilever beams undergoing various large deflections. First, cantilever beam subject to tip loads is analyzed. The tip loads of pure vertical force and pure moment are dealt with, respectively, which represent two extreme load cases. Then, four compliant mechanisms, including a partially compliant four-bar mechanism, a fixed-guided compliant mechanism, a circular-guided mechanism, and a cross-axis flexure pivot, are analyzed and compared to the results of other methods. The first three mechanisms are to show the capabilities of CBCM for modeling deflected flexible beams carrying one or even more inflection points, while the last one is to demonstrate the use of CBCM for compliant mechanisms with more than one flexible beams. In addition, the second mechanism, i.e., the fixed-guided compliant mechanism, also shows the capability of CBCM for accurately predicting the right buckling mode when the axial load is significant. The MATLAB codes of CBCM for all the examples can be downloaded from the website.[3]

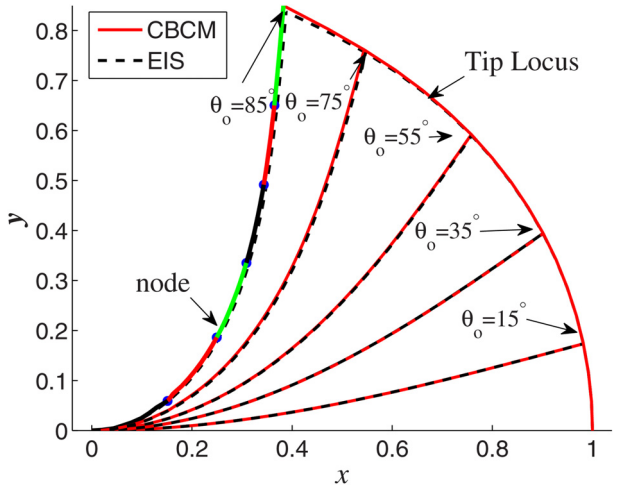

Fig. 3 The beam shape when subjected to pure vertical end force

All the flexible beams being analyzed in the following parts are made of polypropylene, with Young's modulus $E = 1.4 \times 10^9$ Pa. The nonlinear FEA results were obtained using ABAQUS™, with the flexible beam being meshed into 200 elements using quadric beam element B22 and the geometric nonlinearity option turned on.

4.1 Flexible Cantilever Beam Subject to End Loads

4.1.1 Pure Vertical Force. We assume that a pure vertical force is applied. The beam was evenly divided into six elements ($N = 6$) CBCM by dividing it into the deflected configurations achieved by CBCM with $N = 6$ at different tip slopes are shown in Fig. 3. The results of the EIS in Ref. [3] are also plotted for the purpose of comparison. The results of the two methods agree very well. As the tip slope increases, the vertical force tends to stretch the beam. As can be seen from Fig. 3, the tip locus predicted by CBCM apparently goes beyond that obtained by EIS when $\theta_o > 55$ deg, that is to say, CBCM can accurately capture this stretch effect because axial deflections are included in its BCM elements.

4.1.2 Pure End Moment. When the beam subject to a pure moment M_o, according to Bernoulli–Euler beam theory, the curvature of the deformed beam $1/\rho = d\theta/ds = M_o L/EI$ is constant, which means the beam is bent into a circular arc whose radius equals $\rho = EI/M_o L = 1/m_o$ and the deflections can be expressed as

$$\begin{aligned} \theta_o &= m_o \\ X_o &= \frac{\sin(m_o)}{m_o} \\ Y_o &= \frac{1-\cos(m_o)}{m_o} \end{aligned} \tag{16}$$

[3] http://web.xidian.edu.cn/gmchen/files/20150406_131332.rar

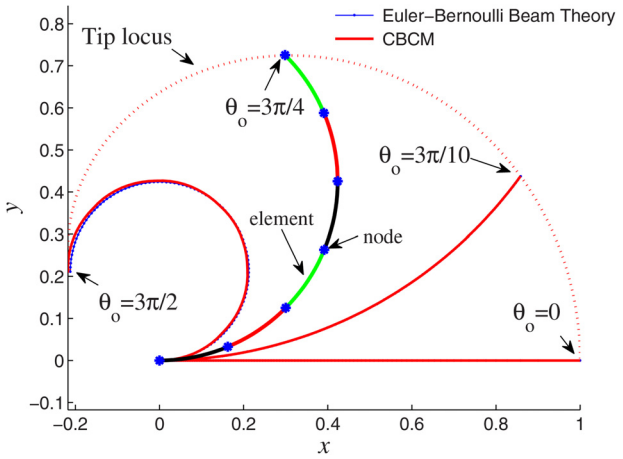

Fig. 4 Deflected configurations when beam subject to an end moment (the stars correspond to the nodes)

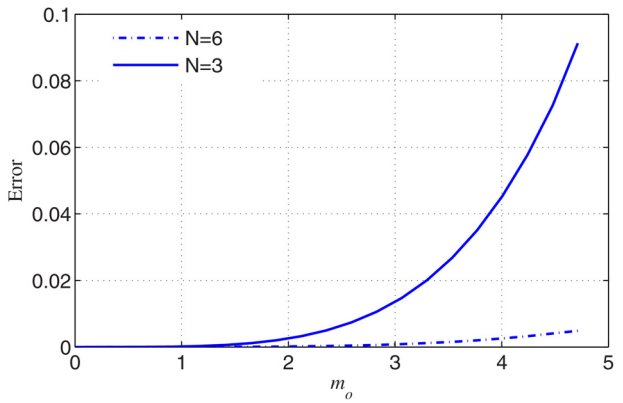

Fig. 5 Tip errors compared to results of Eq. (16)

We modeled the beam using CBCM by evenly dividing it into six elements ($N=6$) and the predicted configurations for m_o varying from 0 to $3\pi/2$ are plotted and compared with the results of the above solution based on Bernoulli–Euler beam theory in Fig. 4. It shows that CBCM with six elements is accurate in a large range of deflection. Figure 5 plots the tip errors (the tip error here is identical to the one defined in Ref. [3]) of the results of CBCM with $N=3$ and $N=6$ compared to the results of Eq. (16). It can be seen from the figure that the tip error of CBCM with $N=3$ dramatically increases as the deflection increases, with the maximum error reaching 9.1% when $\theta_o = 3\pi/2$, while CBCM with $N=6$ cuts this error down to 0.48%.

4.2 Flexible Beams in Compliant Mechanisms. When flexible beams are deflected due to the motion of the compliant mechanism containing them, the tip loads are the unknown parameters. In this case, the kinematic and static equilibrium equations of the mechanism should be incorporated with the CBCM equations of the beams to solve for the deflections of the beams as well as the kinetostatic behaviors of the mechanism. This subsection consists of four compliant mechanisms, each of which contains one or two flexible beams.

4.2.1 Partially Compliant Four-Bar Mechanism. Figure 6 shows a compliant four-bar mechanism taken from Ref. [19]. The parameters of the mechanism are: $L_{DQ} = L_{BC} = L$, $L_{AB} = L + L\cos\theta_2$, $\theta_2 = 3\pi/4$, and $L_{CQ} = L/20$. The kinematic equations are given as

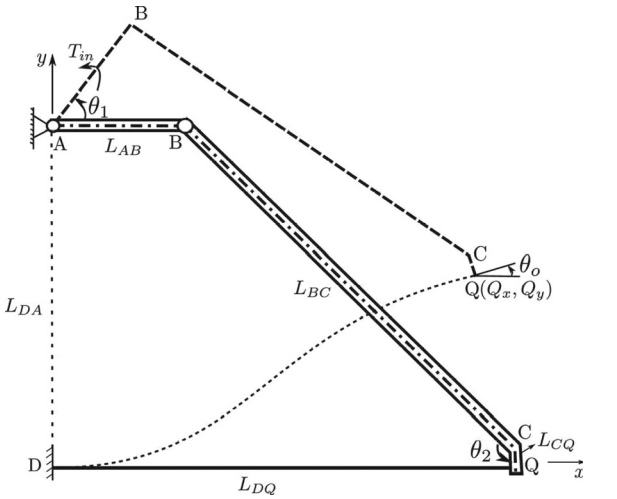

Fig. 6 A partially compliant four-bar mechanism containing a fixed–fixed flexible beam *DQ*

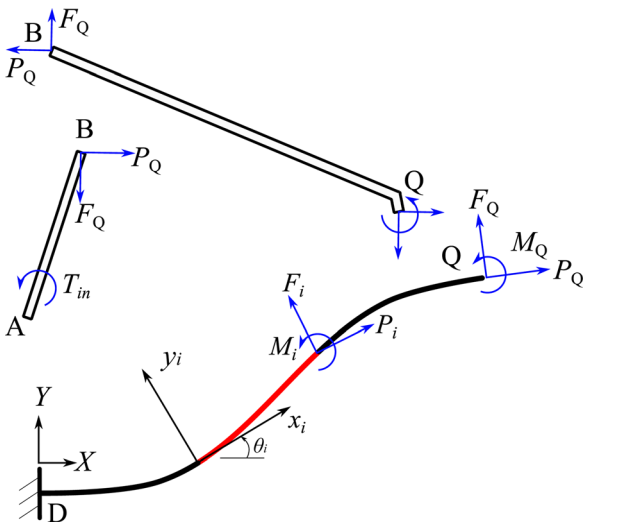

Fig. 7 Free-body diagrams of the mechanism

$$\begin{bmatrix} x_Q \\ y_Q - L_{AD} \end{bmatrix} = \begin{bmatrix} \sin(\theta_0) & \sin(\theta_2 - \theta_0) & \cos(\theta_1) \\ -\cos(\theta_0) & \cos(\theta_2 - \theta_0) & \sin(\theta_1) \end{bmatrix} \begin{bmatrix} L_{CQ} \\ L_{BC} \\ L_{AB} \end{bmatrix} \tag{17}$$

The free-body diagrams of the mechanism subject to a torque T_{in} applied on link AB are shown in Fig. 7. The static equilibrium equations for links AB and BQ can be written as

$$M_Q + F_Q[L_{BC}\sin(\theta_2 - \theta_0) + L_{QC}\sin(\theta_0)] + P_Q[L_{BC}\cos(\theta_2 - \theta_0) - L_{QC}\cos(\theta_0)] = 0 \tag{18}$$

$$T_{\text{in}} = F_Q L_{AB}\cos(\theta_1) + P_Q L_{AB}\sin(\theta_1) \tag{19}$$

We divided the flexible beam DQ into three elements ($N=3$) and established its CBCM equations. The CBCM equations, together with Eqs. (17) and (18), were used to solve for the deflection of the beam and the kinetostatic behaviors of the mechanism for a given crank angle. For the crank angle $\theta_1 \in [0, 2\pi]$, Figs. 8 and 9 plot the obtained kinetostatic curve and strain energy, which indicate that the mechanism is a bistable mechanism. The deflected configurations of the mechanism at $\theta_1 = \pi/4$, $3\pi/4$, $5\pi/4$, and $7\pi/4$ are plotted in Fig. 10. It shows that beam DQ

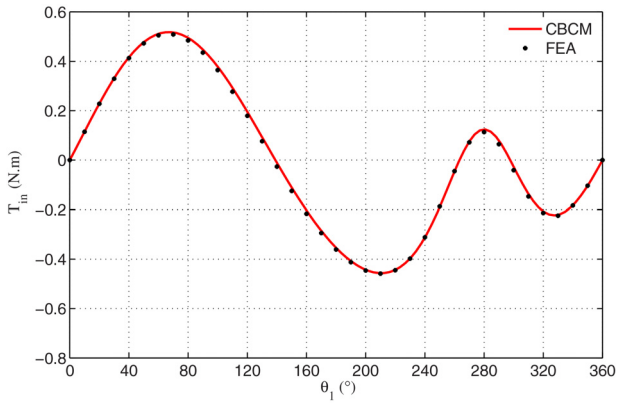

Fig. 8 Force displacement relationship of partial compliant four-bar mechanism

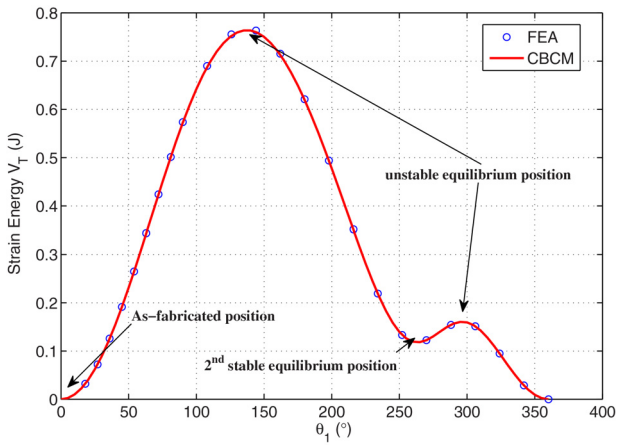

Fig. 9 Strain energy in partially compliant four-bar mechanism

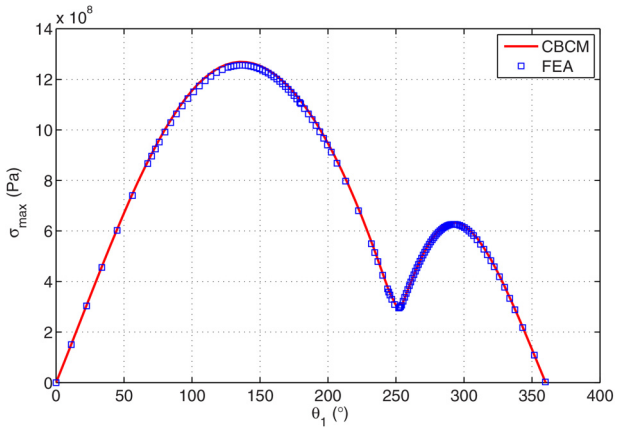

Fig. 11 Maximum stress in partially compliant four-bar mechanism

carries an inflection point at positions $\theta_1 = \pi/4$, $3\pi/4$, and $7\pi/4$. We tried different initial guesses for the parameters, and the model converged to the same solution. The deflected configurations achieved by FEA are plotted as circular dots in Fig. 10. All these figures show that the results obtained by CBCM agree well with the FEA results. The maximum stresses in the mechanism at different positions obtained by CBCM are plotted in Fig. 11, which show a good coincidence with the FEA results. On a personal computer with 3.4 GHz Core i3-2130 processor and memory of 2 GB RAM, it took ABAQUS^{TM} 6.6 s to obtain the results on average, while it took CBCM only 3.6 s to obtain all the results.

4.2.2 Fixed-Guided Compliant Mechanism. The fixed-guided beam *AB* shown in Fig. 12 is a typical compliant segment that has been used in bistable mechanisms and thermal micro-actuators. We place the coordinate frame such that the *x*-axis is along the beam and the origin at point *A*. The beam is modeled using

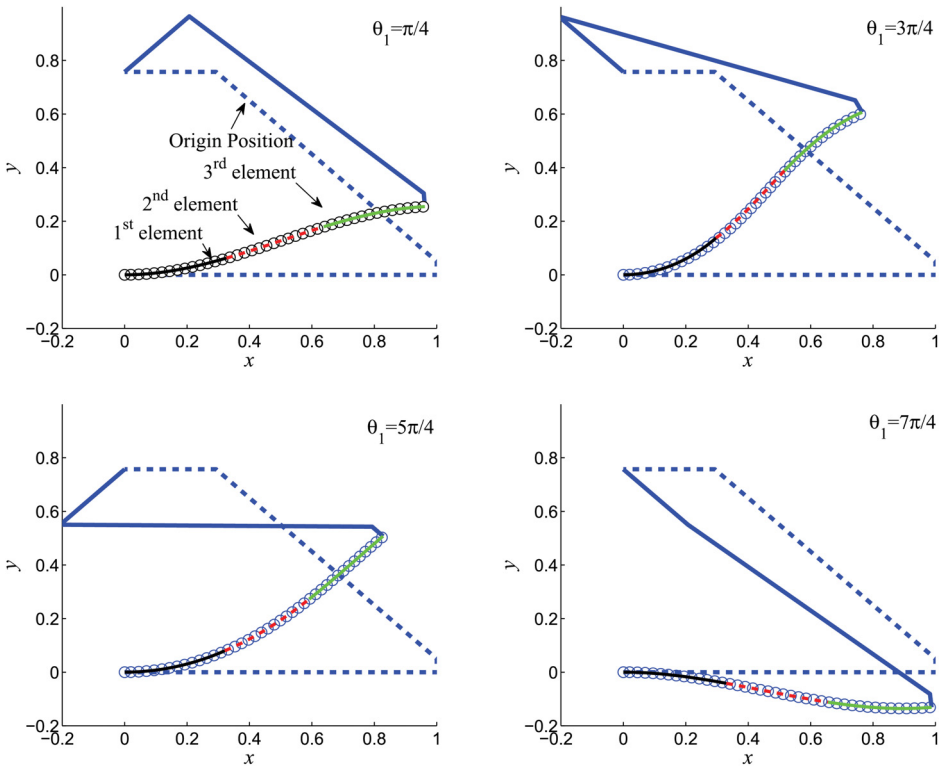

Fig. 10 Deflected configurations of the partial compliant four-bar mechanism at different θ_1

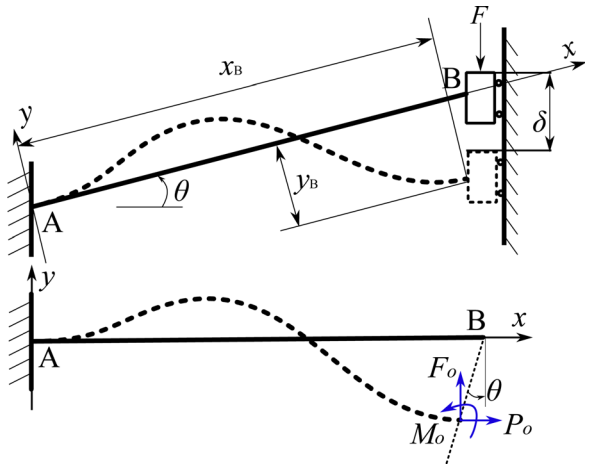

Fig. 12 Diagram of fixed-guided beam

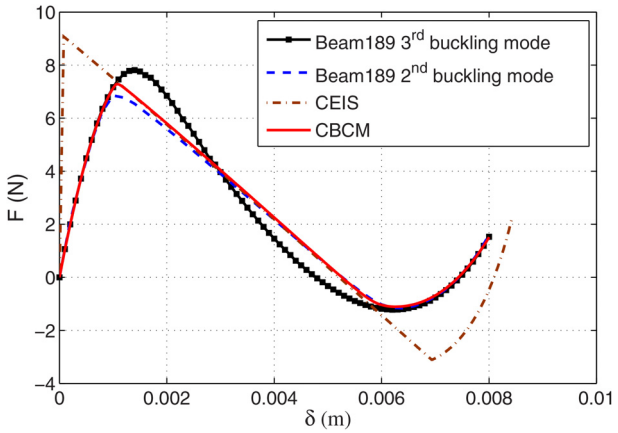

Fig. 14 Force deflection relationships of fixed-guided mechanism

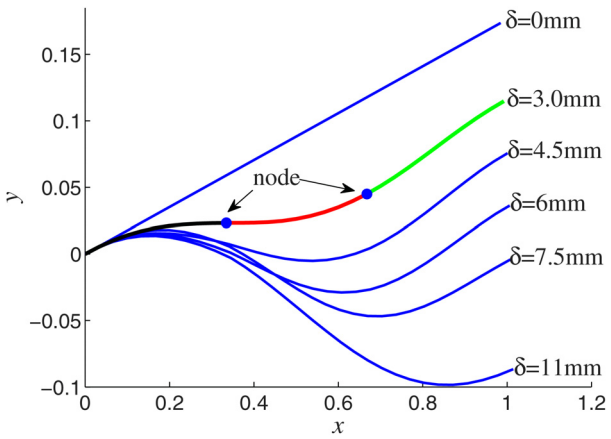

Fig. 13 Deflected configurations of the fixed-guided beam

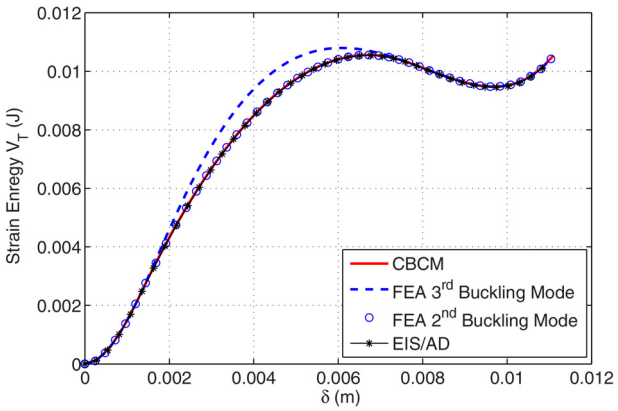

Fig. 15 Comparison of strain energy of the fixed-guided beam

CBCM with $N = 3$. For a given vertical displacement δ at tip B, the corresponding deflection parameters can be written as

$$\begin{aligned} X_o &= L_{AB} - \delta \sin\theta \\ Y_o &= -\delta \cos\theta \\ \theta_o &= 0 \end{aligned} \tag{20}$$

The vertical force F can be expressed by the load parameters (F_o and P_o) as

$$F = F_o \cos\theta + P_o \sin\theta \tag{21}$$

The beam parameters in this example are identical to those used in Ref. [14]: $L_{AB} = 70$ mm, $t = 1.5$ mm, $h = 12.55$ mm, $\theta = 5.5$ deg, and $E = 1.379 \times 10^9$ Pa. Figure 13 plots the deflected configurations of beam obtained by CBCM at different positions. The corresponding force–displacement curve is plotted in Fig. 14. The force–displacement curves obtained by EIS/AD (AD indicates that an axial deflection model is included) [14] and CEIS are also plotted in this figure for the purpose of comparison. CBCM successfully predicted the right deflection modes, as compared to the EIS/AD results. Similar to the results of the bending model only in Ref. [14], CEIS fails to predict the first mode bending occurring at the beginning and end of the force–deflection curve because it neglects axial deflection. The EIS/AD programed in MATLAB [14] spent 2.6 s to obtain the results, while CBCM only used 5.6 s to complete the same calculation.

As being pointed out in Ref. [14], nonlinear FEA models tend to converge to higher buckling modes for this problem, e.g., the third buckling mode shown in Fig. 14. The results of the more realistic second buckling mode (with the first mode bending occurring at the beginning and end of the force–deflection curve) shown in Fig. 14 were obtained by applying a biasing force on the beam in the FEA model. Figures 15 and 16 plot the results for the strain energy curves and the maximum stresses obtained by CBCM and EIS/AD, respectively. The CBCM and EIS/AD results agree well with those of the second buckling mode of the FEA model. The strain energy curve of the third buckling mode obtained by the FEA model shows a higher energy level than that of the more realistic second buckling mode, which concurs the prediction presented in Ref. [7].

4.2.3 Circular-Guided Compliant Mechanism. Consider the circular-guided compliant mechanism taken from Ref. [7]. As shown in Fig. 17, an driving torque T_{in} is applied to rigid link BA and the tip of flexible link OA follows a circle. The parameters of the flexible beam and the mechanism are listed in Table 2. The deflection parameters of OA for a given rigid-link angle β can be expressed as

$$\begin{aligned} X_o &= L_{OA} - L_{BA} + L_{BA}\cos(\beta) \\ Y_o &= L_{BA}\sin(\beta) \\ \theta_o &= \beta \end{aligned} \tag{22}$$

We modeled the flexible beam using CBCM with $N = 7$ (seven elements) and solved the CBCM equations for the load parameters

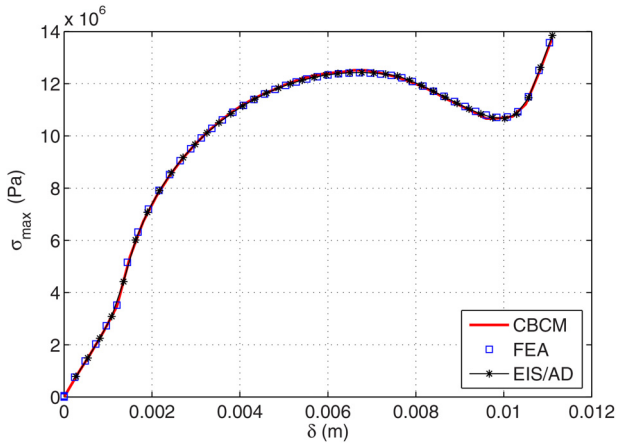

Fig. 16 Maximum stress along the fixed-guided beam

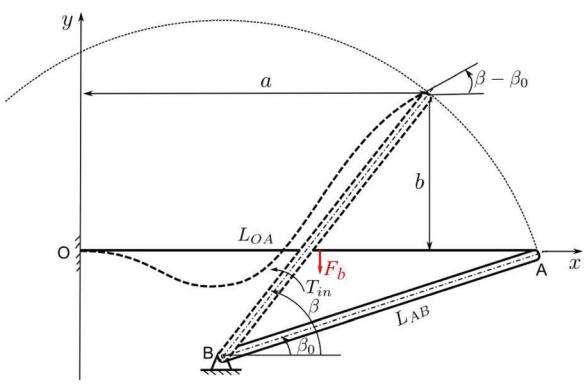

Fig. 17 Circular-guided compliant mechanism

Table 2 Parameters of circular-guided mechanism

L_{AB} (mm)	L_{OA} (mm)	β_0(deg)	h (mm)	w (mm)
30	20	30	6	1.2

using the deflection parameters given by Eq. (22). Figure 18 plots the driving torque as a function of the crank angle $\beta \in [\pi/6, \pi/2]$, in which the driving torque was calculated using the obtained load parameters as

$$T_{\text{in}} = F_o L_{AB} \cos\beta + P_o L_{AB} \sin\beta + M_o \tag{23}$$

The deflected configurations of OA at different values of β are plotted in Fig. 19. It shows that the deflected OA contains two inflection points. The corresponding results of the CEIS [7] are also plotted in Figs. 18 and 19 for the purpose of comparison. The results of CBCM show a good coincidence with the CEIS results, and the maximum error of the driving torques predicted by the two methods is 1.75% occurring at $\beta = 90$ deg. It took CEIS 1.5 s to obtain the results, while it took CBCM 5.6 s to complete the calculation. Due to its closed-form expressions, CEIS is usually more efficient than CBCM.

Similar to the previous problem, the nonlinear FEA model for the circular-guided mechanism tends to converge to a higher buckling mode, as shown in Fig. 19. In order to correct the buckling mode, a biasing force $F_b = 0.1N$ was applied at the center of beam OA, as illustrated in Fig. 17. Figure 19 also plots the corrected deflected configuration at position $\beta = \pi/2$, which agrees well with the deflected configurations achieved by CBCM and CEIS. The strain energy curve and the maximum stresses obtained

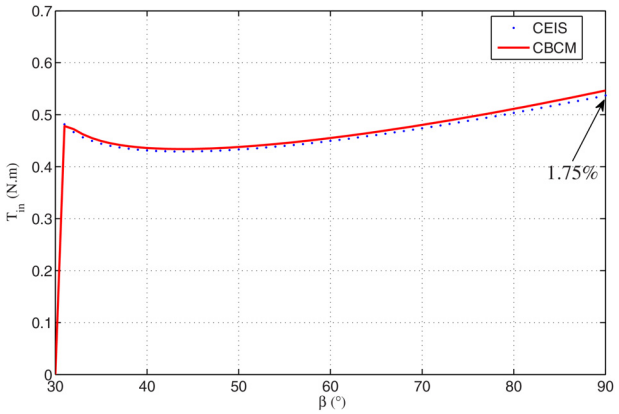

Fig. 18 Kinetostatic behavior of circular-guided mechanism

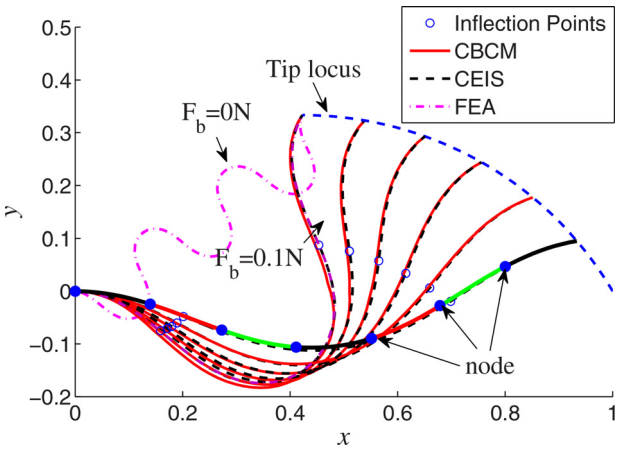

Fig. 19 Deflected configurations of circular-guided mechanism

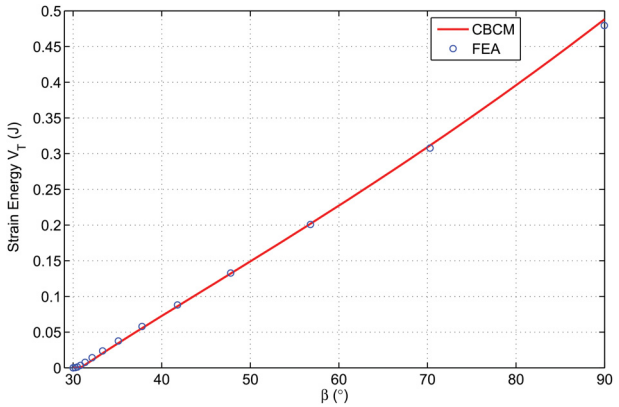

Fig. 20 Strain energy stored in circular-guided mechanism

by the corrected FEA model were used to validate those of CBCM, as shown in Figs. 20 and 21. The results are in good agreement.

4.2.4 Cross-Axis Flexural Pivot. As shown in Fig. 22, a cross-axis flexural pivot contains two flexible beams of equal length ($L_{O_1A} = L_{O_2B} = L$) oriented symmetrically about the Y-axis. The angle between the two members is 2β. Point C is the midpoint of rigid part AB. Let $L_{O_1O_2} = w_1, L_{AB} = w_2$, and $N_o = w_1/w_2$, and we have

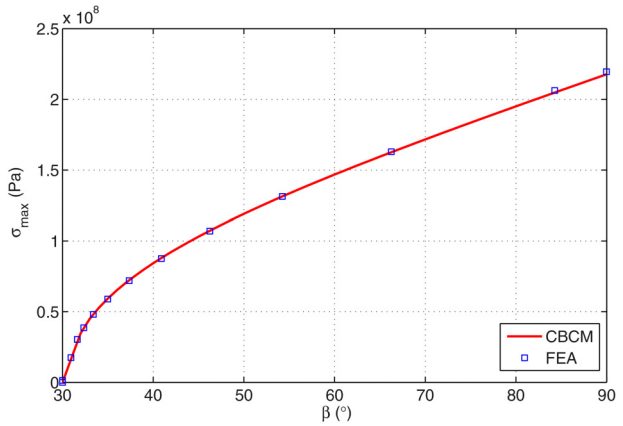

Fig. 21 Maximum stress on flexible beam in circular-guided mechanism

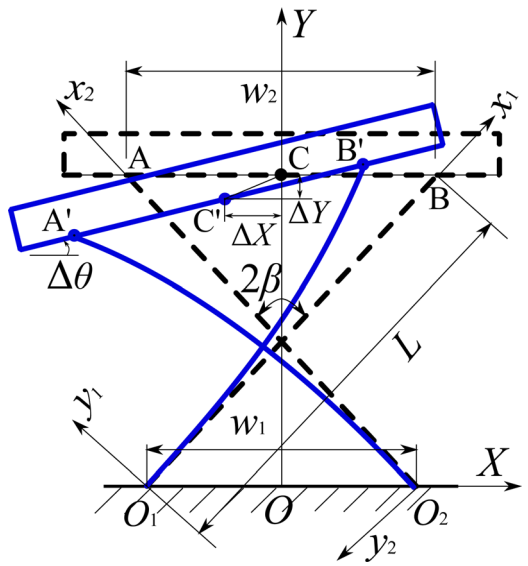

Fig. 22 Geometry of cross-axis flexural pivot

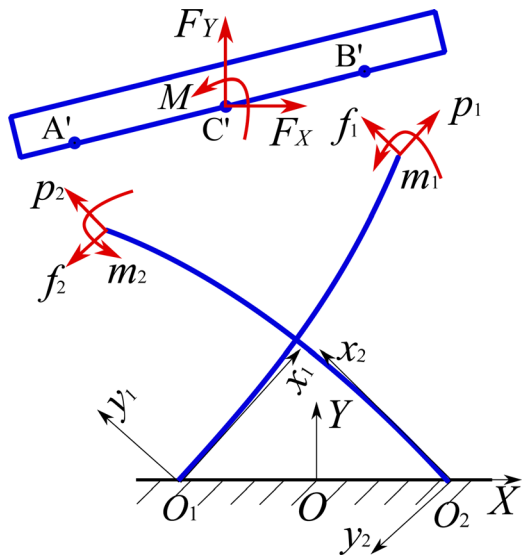

Fig. 23 Free-body diagrams of cross-axis flexural pivot

Table 3 Geometric parameters of cross-axis flexural pivot

L (mm)	N_o	β(deg)	h (mm)	w (mm)
60	4	60	25.2	1

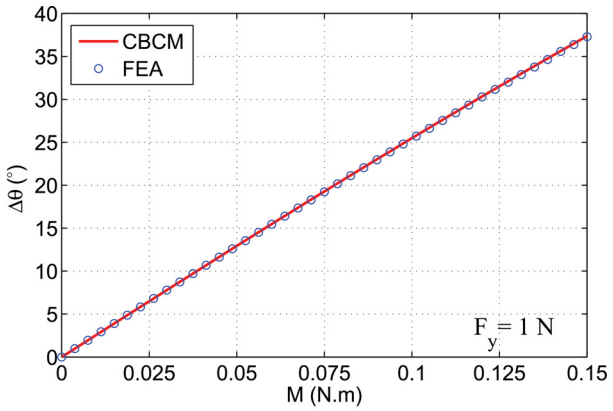

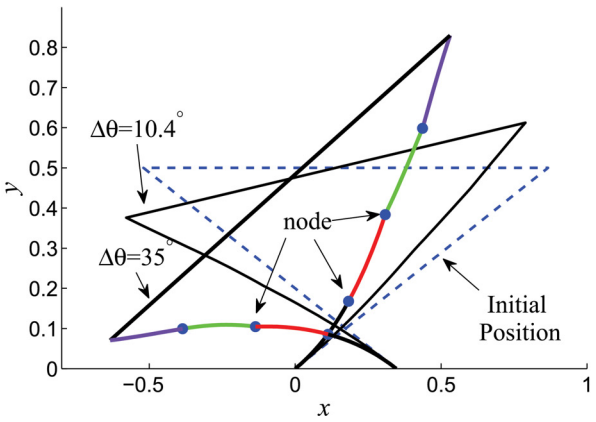

Fig. 24 Kinetostatic behaviors and deflected configurations of cross-axis flexural pivot

$$w_1 = 2L\sin\beta/(N+1)$$
$$w_2 = 2NL\sin\beta/(N+1) \tag{24}$$

The displacements of rigid part AB after the pivot being deflected can be given as

$$\Delta\theta = \theta_{o1} = \theta_{o2}$$
$$\begin{bmatrix}\Delta X\\ \Delta Y\end{bmatrix} = \frac{1}{2}\begin{bmatrix}\cos\beta & \sin\beta\\ -\sin\beta & \cos\beta\end{bmatrix}\begin{bmatrix}-(Y_A+Y_B) & Y_A-Y_B\\ -(X_A-X_B) & X_A+X_B\end{bmatrix} \tag{25}$$

where θ_{o1} and θ_{o2} are the tip slopes of the O_1A and O_2B with respect to coordinate frames $x_1O_1y_1$ and $x_2O_2y_2$, respectively. The loop closure equations can be written as

$$\begin{bmatrix}\sin\beta & -\cos\beta\\ \cos\beta & \sin\beta\end{bmatrix}\begin{bmatrix}X_B\\ Y_B\end{bmatrix} = \begin{bmatrix}-\sin\beta & -\cos\beta\\ \cos\beta & -\sin\beta\end{bmatrix}\begin{bmatrix}X_A\\ Y_A\end{bmatrix} + \begin{bmatrix}w_1+w_2\cos(\Delta\theta)\\ w_2\sin(\Delta\theta)\end{bmatrix} \tag{26}$$

The static equilibrium equations are written as (as shown in Fig. 23)

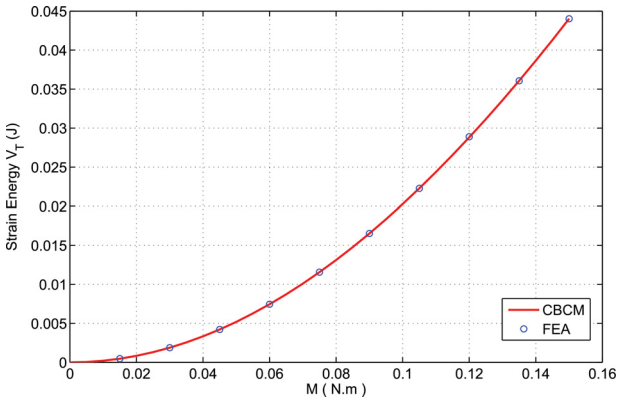

Fig. 25 Comparison of strain energy in cross-axis flexural pivot

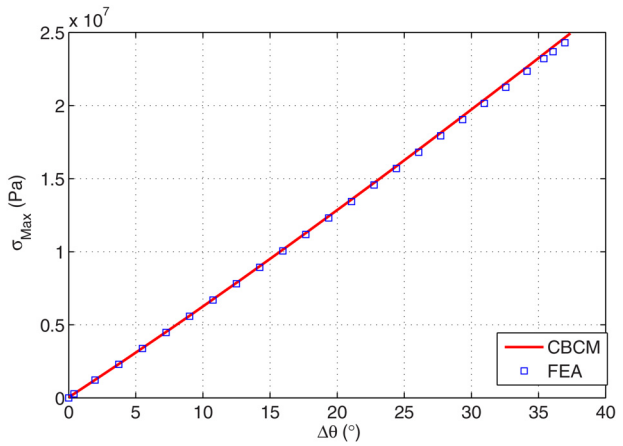

Fig. 26 Maximum stress of the total mechanism

$$M = m_1 + m_2 + w_2[-\sin(\Delta\theta)\ \ \cos(\Delta\theta)]\begin{bmatrix}\sin\beta & \cos\beta\\ -\cos\beta & \sin\beta\end{bmatrix} \times \begin{bmatrix}p_2\\ f_2\end{bmatrix} + \frac{1}{2}w_2[\sin(\Delta\theta) - \cos(\Delta\theta)]\begin{bmatrix}F_X\\ F_Y\end{bmatrix}$$

$$\begin{bmatrix}F_X\\ F_Y\end{bmatrix} = \begin{bmatrix}-\sin\beta & \cos\beta\\ -\cos\beta & -\sin\beta\end{bmatrix}\begin{bmatrix}p_1\\ f_1\end{bmatrix} + \begin{bmatrix}\sin\beta & \cos\beta\\ -\cos\beta & \sin\beta\end{bmatrix}\begin{bmatrix}p_2\\ f_2\end{bmatrix} \tag{27}$$

Table 3 lists the geometric parameters of the flexural pivot. Both flexible beams were modeled using CBCM with $N = 4$ (four elements). Applying a gradually increased moment and a constant vertical force ($F_y = 1$ N) at point C, the loop closure and static equilibrium equations given above, together with the CBCM equations of both flexible beams, were solved for the kinetostatic behaviors of the flexural pivot. Figure 24 plots the rotation angle of the rigid part as a function of the applied moment and the deflected configurations at different positions. Figure 24 also plots the FEA results. The results obtained by both methods are in good consistent in a large range of rotation ($\Delta\theta$ up to 40 deg). In contrast, the BCM-based model for similar flexural pivots [13] is accurate only for the rotation angle less than 20 deg. Figures 25 and 26 show that both the strain energy and the maximum stress predicted by CBCM and the FEA model are in good agreement. On a personal computer with 3.4 GHz Core i3-2130 processor and memory of 2 GB RAM, it took ABAQUS™ 8.5 s to obtain the results, while CBCM (implemented in MATLAB) consumed 3.7 s to complete all the calculation.

5 Conclusions

In this work, an alternative method for modeling large deflections called CBCM was proposed by extending BCM through segmentation. The examples demonstrated that CBCM is capable of solving various deflection problems of flexible beams in compliant mechanisms. Due to their closed-form solutions, EIS/AD and CEIS are usually more efficient than CBCM. CBCM requires much fewer elements than other discretization-based methods utilizing linear elements (e.g., the chain algorithm and the circle-arc method) to obtain desired accuracy. Because axial deflections are included in BCM elements, CBCM outperforms the methods that neglect axial deflections (e.g., CEIS) for modeling flexible beams subject to axial-force dominated loads. Although a modified FEA model can predict the right buckling mode of flexible beam subject to axial-force dominated loads by applying an unrealistic biasing force [14] or altering the model parameters [26], these modifications should always be carefully handled to minimize the errors due to the modifications.

The minimum number of BCM elements (denoted as N_s) required for CBCM to achieve results with satisfactory accuracy can be determined using the following rules of thumb: (i) for large deflections without inflection points, $Ns = \lceil \max(4\theta_m/\pi, 8Y_{om}/L) \rceil$, where θ_m and Y_{om} are the maximum values of the tip slope and the vertical tip deflection, respectively, and $\lceil \cdot \rceil$ denotes the ceiling function; (ii) for deflections carry one or more inflection points, $Ns = \lceil \max(n_i, |2p_m|/\pi) \rceil$, where n_i represents the number of the inflection points, and p_m is the maximum value of the axial force. Generally, utilizing more BCM elements can always increase the modeling accuracy of CBCM.

Acknowledgment

The authors gratefully acknowledge Professor Brian D. Jensen for providing the MATLAB code of EIS/AD. The financial supports from the National Natural Science Foundation of China under Grant No. 51175396, the Specialized Research Fund for the Doctoral Program of Higher Education of China under Grant No. 20120203110015, and the Fundamental Research Funds for the Central Universities under No. K5051204021 are also acknowledged.

References

[1] Slocum, A. H., 1992, *Precision Machine Design*, Society of Manufacturing Engineers, Dearborn, MI.
[2] Smith, S. T., 2000, *Flexures: Elements of Elastic Mechanisms*, Gordon and Breach Science, New York.
[3] Howell, L. L., 2001, *Compliant Mechanisms*, Wiley, New York.
[4] Chen, G., and Du, Y., 2012, "Double-Young Tristable Mechanisms (DYTMs)," ASME J. Mech. Rob., **5**(1), p. 011007.
[5] Blanding, D. L., 1999, *Exact Constraint: Machine Design Using Kinematic Processing*, ASME, New York.
[6] Morsch, F. M., Tolou, N., and Herder, J. L., 2009, "Comparison of Methods for Large Deflection Analysis of a Cantilever Beam Under Free End Point Load Cases," ASME Paper No. DETC2009-86754.
[7] Zhang, A., and Chen, G., 2013, "A Comprehensive Elliptic Integral Solution to the Large Deflection Problems of Thin Beams in Compliant Mechanisms," ASME J. Mech. Rob., **5**(2), p. 021006.
[8] Campanile, L. F., and Hasse, A., 2008, "A Simple and Effective Solution of the Elastica Problem," Proc. Inst. Mech. Eng., Part C, **222**(12), pp. 2513–2516.
[9] Tolou, N., and Herder, J. L., 2009, "A Semianalytical Approach to Large Deflections in Compliant Beams Under Point Load," Math. Probl. Eng., **2009**(2009), p. 910896.
[10] Banerjee, A., Bhattacharya, B., and Mallik, A. K., 2008, "Large Deflection of Cantilever Beams With Geometric Non-Linearity: Analytical and Numerical Approaches," Int. J. Non-Linear Mech., **43**(5), pp. 366–376.
[11] Midha, A., Her, I., and Salamon, B., 1992, "Methodology for Compliant Mechanisms Design. Part I—Introduction and Large-Deflection Analysis," 18th ASME Design Automation Conference, Scottsdale, AZ, Sept. 13–16.
[12] Awtar, S., Slocum, A. H., and Sevincer, E., 2007, "Characteristics of Beam-Based Flexure Modules," ASME J. Mech. Des., **129**(6), pp. 625–639.
[13] Bi, S., Zhao, H., and Yu, J., 2009, "Modeling of a Cartwheel Flexural Pivot," ASME J. Mech. Des., **131**(6), p. 061010.

[14] Holst, G. L., Teichert, G. H., and Jensen, B. D., 2013, "Modeling and Experiments of Buckling Modes and Deflection of Fixed-Guided Beams in Compliant Mechanisms," ASME J. Mech. Des., **133**(5), p. 051002.
[15] Chen, G., and Ma, F., 2015, "Kinetostatic Modeling of Fully Compliant Bistable Mechanisms Using Timoshenko Beam Constraint Model," ASME J. Mech. Des., **137**(2), p. 022301.
[16] Timoshenko, S. P., 1940, *Strength of Materials*, 2nd ed., D. Van Nostrand Company, New York.
[17] Hearn, E. J., 1977, *Mechanics of Materials*, Pergamon Press, Oxford, UK.
[18] Kimball, C., and Tsai, L. W., 2002, "Modeling of Flexural Beams Subjected to Arbitrary End Loads," ASME J. Mech. Des., **124**(2), pp. 223–235.
[19] Su, H. J., 2009, "A Pseudorigid-Body 3R Model for Determining Large Deflection of Cantilever Beams Subject to Tip Loads," ASME J. Mech. Rob., **1**(2), p. 021008.
[20] Chen, G., Xiong, B., and Huang, X., 2011, "Finding the Optimal Characteristic Parameters for 3R Pseudo-Rigid-Body Model Using an Improved Particle Swarm Optimizer," J. Int. Soc. Precis. Eng. Nanotechnol., **35**(3), pp. 505–511.
[21] Chen, G., and Zhang, A., 2011, "Accuracy Evaluation of PRBM for Predicting Kinetostatic Behavior of Flexible Segments in Compliant Mechanisms," ASME Paper No. DETC2011-47117.
[22] Saxena, A., and Kramer, S. N., 1998, "A Simple and Accurate Method for Determining Large Deflections in Compliant Mechanisms Subjected to End Forces and Moments," ASME J. Mech. Des., **120**(3), pp. 392–400.
[23] Lan, C. C., 2008, "Analysis of Large-Displacement Compliant Mechanisms Using an Incremental Linearization Approach," Mech. Mach. Theory, **43**(5), pp. 641–658.
[24] Awtar, S., Shimotsu, K., and Sen, S., 2010, "Elastic Averaging in Flexure Mechanisms: A Three-Beam Parallelogram Flexure Case Study," ASME J. Mech. Rob., **2**(4), p. 041006.
[25] Awtar, S., and Sen, S., 2010, "A Generalized Constraint Model for Two-Dimensional Beam Flexures: Nonlinear Strain Energy Formulation," ASME J. Mech. Des., **132**(8), p. 081009.
[26] Dunning, A. G., Tolou, N., Pluimers, P. P., Kluit, L. F., and Herder, J. L., 2012, "Bistable Compliant Mechanisms: Corrected Finite Element Modeling for Stiffness Tuning and Preloading Incorporation," ASME J. Mech. Des., **134**(8), p. 084502.